William & Mary
CHARTERED 1693

W&M ScholarWorks

VIMS Articles

Virginia Institute of Marine Science

2019

High-frequency CO2-system variability over the winter-to-spring transition in a large coastal plain estuary

Elizabeth H. Shadwick
Virginia Institute of Marine Science

Marjorie A.M. Friedrichs
Virginia Institute of Marine Science

Raymond G. Najjar

Olivia A. De Meo
Virginia Institute of Marine Science

Jaclyn R. Friedman
Virginia Institute of Marine Science

See next page for additional authors

Follow this and additional works at: https://scholarworks.wm.edu/vimsarticles

 Part of the Oceanography Commons

Recommended Citation

Shadwick, Elizabeth H.; Friedrichs, Marjorie A.M.; Najjar, Raymond G.; De Meo, Olivia A.; Friedman, Jaclyn R.; Da, Fei; and Reay, W. G., High-frequency CO2-system variability over the winter-to-spring transition in a large coastal plain estuary (2019). *Journal of Geophysical Research: Oceans*, 124(11), 7626-7642. 10.1029/2019JC015246

This Article is brought to you for free and open access by the Virginia Institute of Marine Science at W&M ScholarWorks. It has been accepted for inclusion in VIMS Articles by an authorized administrator of W&M ScholarWorks. For more information, please contact scholarworks@wm.edu.

Authors

Elizabeth H. Shadwick, Marjorie A.M. Friedrichs, Raymond G. Najjar, Olivia A. De Meo, Jaclyn R. Friedman, Fei Da, and W. G. Reay

This article is available at W&M ScholarWorks: https://scholarworks.wm.edu/vimsarticles/1796

JGR Oceans

RESEARCH ARTICLE
10.1029/2019JC015246

Special Section:
Carbon cycling in tidal wetlands and estuaries of the contiguous United States

High-Frequency CO_2 System Variability Over the Winter-to-Spring Transition in a Coastal Plain Estuary

Elizabeth H. Shadwick[1,2], Marjorie A. M. Friedrichs[2], Raymond G. Najjar[3], Olivia A. De Meo[2], Jaclyn R. Friedman[2], Fei Da[2], and William G. Reay[2]

[1]CSIRO Oceans & Atmosphere, Hobart, Tasmania, Australia, [2]Virginia Institute of Marine Science, William & Mary, Gloucester Point, VA, USA, [3]The Pennsylvania State University, University Park, PA, USA

Key Points:
- Several transitions from autotrophy to heterotrophy were observed
- The region is not easily characterized by a spring bloom followed by summer production and winter respiration
- Winter-to-spring transitions in dissolved inorganic carbon are dominated by circulation and biology

Correspondence to:
E. H. Shadwick,
elizabeth.shadwick@csiro.au

Citation:
Shadwick, E. H., Friedrichs, M. A. M., Najjar, R. G., De Meo, O. A., Friedman, J. R., Da, F., & Reay, W. G. (2019). High-frequency CO_2 system variability over the winter-to-spring transition in a coastal plain estuary. *J. Geophys. Res. Oceans*, *124*. https://doi.org/10.1029/2019JC015246

Received 29 APR 2019
Accepted 9 SEP 2019
Accepted article online 13 SEP 2019

©2019. The Authors.
This is an open access article under the terms of the Creative Commons Attribution-NonCommercial-NoDerivs License, which permits use and distribution in any medium, provided the original work is properly cited, the use is non-commercial and no modifications or adaptations are made.

Abstract Understanding the vulnerability of estuarine ecosystems to anthropogenic impacts requires a quantitative assessment of the dynamic drivers of change to the carbonate (CO_2) system. Here we present new high-frequency pH data from a moored sensor. These data are combined with discrete observations to create continuous time series of total dissolved inorganic carbon (TCO_2), CO_2 partial pressure (pCO_2), and carbonate saturation state. We present two deployments over the winter-to-spring transition in the lower York River (where it meets the Chesapeake Bay mainstem) in 2016/2017 and 2017/2018. TCO_2 budgets with daily resolution are constructed, and contributions from circulation, air-sea CO_2 exchange, and biology are quantified. We find that TCO_2 is most strongly influenced by circulation and biological processes; pCO_2 and pH also respond strongly to changes in temperature. The system transitions from autotrophic to heterotrophic conditions multiple times during both deployments; the conventional view of a spring bloom and subsequent summer production followed by autumn and winter respiration may not apply to this region. Despite the dominance of respiration in winter and early spring, surface waters were undersaturated with respect to atmospheric CO_2 for the majority of both deployments with mean fluxes ranging from −9 to −5 mmol $C \cdot m^{-2} \cdot day^{-1}$. Deployments a year apart indicate that the seasonal transition in the CO_2 system differs significantly from one year to the next and highlights the necessity of sustained monitoring in dynamic nearshore environments.

1. Introduction

The carbonate chemistry of estuarine environments is currently being impacted by a complex suite of anthropogenic stressors, including the impact of rising atmospheric carbon dioxide (CO_2), warming, and sea-level rise. During the past century, the oceanic uptake of ~30% of the anthropogenic CO_2 emissions has decreased the open-ocean surface pH by 0.1 units and the carbonate ion concentration by 10% (Doney et al., 2009; Feely et al., 2009; Orr et al., 2005). The magnitude of this acidification effect in estuarine systems is less well constrained (Duarte et al., 2013; Wallace et al., 2014) but may be more prominent in lower-salinity waters (Waldbusser & Salisbury, 2014), particularly those impacted by eutrophication (Borges & Gypens, 2010; Wallace et al., 2014).

Eutrophication has long been known to lead to excessive production of organic matter and a corresponding increase in microbial respiration, which not only reduces oxygen in bottom waters but also decreases pH through the concomitant production of CO_2 (Cai, 2011; Feely et al., 2010; Sunda & Cai, 2012). The nonpristine estuaries of the U.S. East coast have been identified as vulnerable regions due to the emergence of multiple environmental stressors, including eutrophication and hypoxia, and their impacts on shellfish populations and human communities that depend on the shellfish industry (Ekstrom et al., 2015). Over the past decade, the volume of seasonally hypoxic water in the Chesapeake Bay has not shown a clear decrease in response to ongoing nutrient reductions (Bever et al., 2013; Du et al., 2018). Enhanced respiration at depth not only leads to the generation of hypoxic conditions but also decreased pH through the production of CO_2, potentially exacerbating acidification in the estuary.

The dynamic nature of estuarine environments results in important interactions between physical and biological forcing, which influence variability in the carbonate chemistry (e.g., Flecha et al., 2015; Joesoef et al., 2017; Salisbury & Jönsson, 2018). Capturing high-frequency events is challenging with traditional shipboard sampling, and many of the pH time series from coastal systems come from fixed platforms as part of regional

water quality monitoring efforts (e.g., the National Estuarine Research Reserve System in the United States). Understanding acidification requires measurement of (at least) two CO_2 system parameters (Goldsmith et al., 2019). Recent work has shown the utility of using autonomous sensors to obtain high-frequency pH observations (e.g., Gonski et al., 2018; Hofmann et al., 2011; Martz et al., 2014; Shadwick et al., 2015; Sutton et al., 2014; Takeshita et al., 2015). We present new data from a moored pH sensor complimented by discrete sampling of total dissolved inorganic carbon and alkalinity, which allows for robust pH sensor calibration and an extension of the moored time series to the full CO_2 system with daily resolution. Observations from two sensor deployments of several months duration during the winter-to-spring transition at the confluence of the York River and the Chesapeake Bay mainstem are presented. These observations are used to construct an inorganic carbon budget and partition the changes into physical and biological drivers.

2. Study Site

The York River is the fifth largest tributary in the Chesapeake Bay system in terms of both flow and watershed area (Reay, 2009). We present observations from the lower York River, where it joins the mainstem of the Chesapeake Bay (Figure 1). The York River is classified as a microtidal, partially mixed, estuary with a mean tidal range of 0.7 m and polyhaline ($18 < \text{salinity} < 30$) conditions in its lower portion. Stability of the water column is controlled by freshwater inputs as well as local surface heating (Sharples et al., 1994). There is decreased turbulent mixing during neap tide conditions, and stratification has been shown to regularly oscillate with the spring-neap tidal cycle in the lower York River system (Haas, 1977).

The York River experiences numerous water quality issues, including eutrophication, hypoxia, and harmful algal blooms, all of which are tied to the highly seasonal nature of the system. Riverine input plays a particularly important role, with pelagic gross primary production positively correlated with discharge and total nitrogen load (Qin & Shen, 2019). A phytoplankton bloom usually occurs in the spring with biomass typically dominated by diatoms and associated with the input of riverine nutrients (Marshall et al., 2006; Reay, 2009). The decline of the spring bloom results in recycled production with greater phytoplankton community diversity, and biomass continues to decline through the autumn and winter due to reduced light availability and decreasing water temperature (Kemp & Boynton, 1992). Enhanced stratification resulting from spring discharge can lead to the development of low-oxygen conditions in the subsurface waters (Lin & Kuo, 2001; Reay, 2009). Sporadic, and at times extensive, harmful algal blooms, most notably the dinoflagellate *Margalefidinium polykrikoides* (formerly *Cochlodinium polykrikoides*), have occurred within the lower York River for decades (Marshall, 2009).

Although the Chesapeake Bay mainstem and its tributaries have been well studied in terms of nutrient loading and subsequent eutrophication and hypoxia (e.g., Boynton et al., 1995; Da et al., 2018; Irby & Friedrichs, 2019; Kemp, 2005; Kemp et al., 1997), the carbonate chemistry of the region is less well understood (Raymond et al., 2000; Waldbusser et al., 2011; Wong, 1979), though focused observational and modeling studies are emerging (Brodeur et al., 2019; Cai et al., 2017; Shen et al., 2019). The mainstem of the Chesapeake Bay is thought to be net autotrophic on the annual scale, while its tributaries are thought to be net heterotrophic (Feng et al., 2015; Herrmann et al., 2015; Kemp et al., 1997; Najjar et al., 2018); the mainstem Bay as a whole likely acts as a sink for atmospheric CO_2 (Brodeur et al., 2019; Shen et al., 2019).

3. Methods

The primary CO_2 system measurements include continuous pH and discrete total dissolved inorganic carbon (TCO_2) and total alkalinity (TA) at the York River Buoy, as well as discrete TCO_2 and TA at a nearby station of the Chesapeake Bay Water Quality Monitoring Program. The continuous pH measurements are placed into context via an analysis of long-term discrete pH data from the monitoring station. The continuous pH data are also used to generate continuous time series of TCO_2, TA, CO_2 partial pressure (pCO_2), and aragonite saturation state (Ω_{ar}). Changes in these CO_2 system variables are partitioned into changes resulting from exchange with the atmosphere, changes in temperature, circulation, and biological processes.

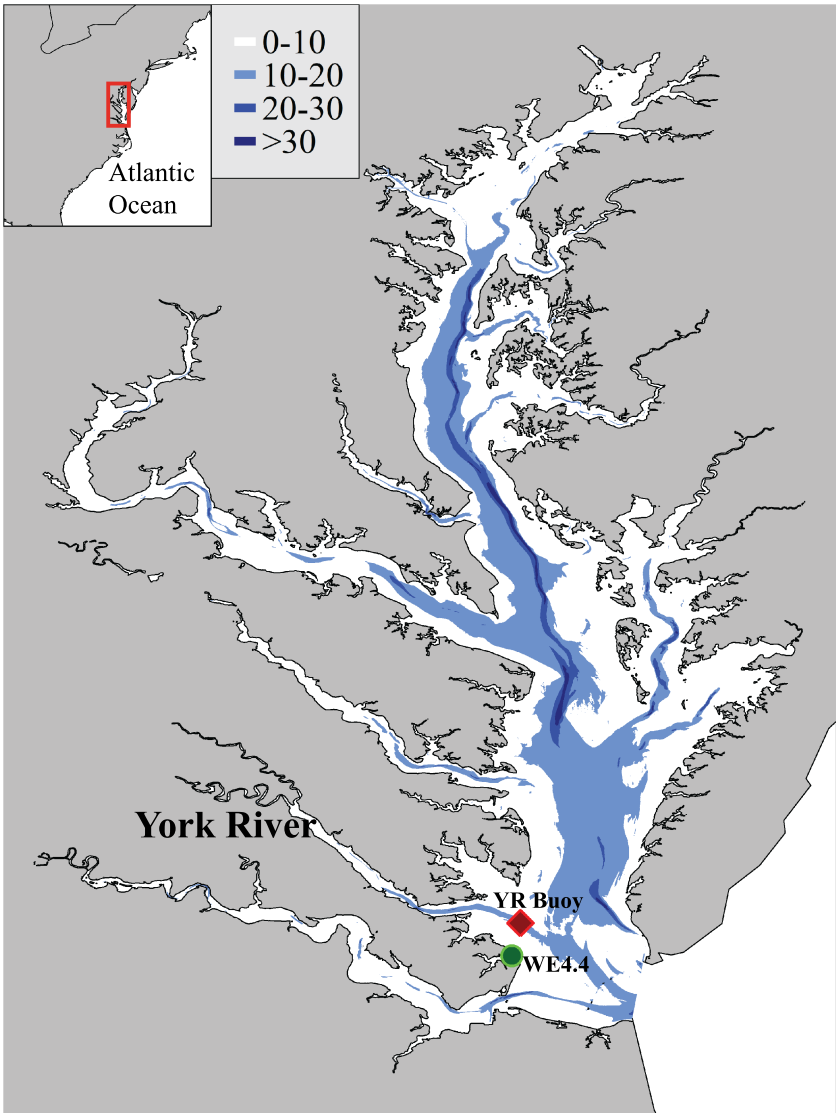

Figure 1. Locations of the Chesapeake Bay Interpretive Buoy System York River Buoy (red diamond) at the confluence of the York River and the Chesapeake Bay mainstem and the long-term water quality monitoring Station WE4.4 (green circle).

3.1. High-Frequency Observations

A SeapHOx sensor was deployed at the National Oceanic and Atmospheric Administration Chesapeake Bay Interpretive Buoy System (https://buoybay.noaa.gov/) York River Buoy (latitude: 37.20°N, longitude 76.27° W; Figure 1) with roughly 8-m water depth. The sensor was placed in a custom-built stainless steel frame and suspended from the surface buoy, with the instrument intake depth approximately 1.5 m below the water surface. The SeapHOx uses an integrated sensor package that consists of a Sea-Bird SBE-37 conductivity and temperature sensor, an Aanderaa oxygen optode, and a modified Honeywell Durafet pH electrode (Bresnahan et al., 2014; Martz et al., 2010). Data are acquired from a pumped flow stream with hourly resolution. We present two deployments: Deployment 1 (D1) between November 2016 and April 2017 and Deployment 2 (D2) between December 2017 and June 2018. This analysis is focused on the transition from winter to spring, and while sensor data were acquired at hourly resolution, we focused the analysis presented here on lower-frequency data, averaged over a 24-hr period.

3.2. Discrete Total CO_2 and Alkalinity Observations

Discrete samples for TCO_2 and TA were collected from the York River buoy and a nearby station of the Chesapeake Bay Water Quality Monitoring Program (Station WE4.4, 10 km from the buoy). Buoy samples were collected alongside the sensor at the beginning and end of each deployment and when possible throughout the deployment (n=8; see Figure 2), following recommended best practices (Bresnahan et al., 2014). Samples were collected at the surface following Chesapeake Bay Program protocols at StationWE4.4 in November 2016, April 2017, January 2018, and April 2018. At both sites, samples were collected in borosilicate glass bottles. The York River buoy samples were stored on ice and in the dark and fixed with a solution of supersaturated mercuric chloride ($HgCl_2$) upon return to the laboratory 1 to 4 hr after sample collection. Samples from the WE4.4 were fixed with $HgCl_2$ immediately after collection. TCO_2 was analyzed by nondispersive infrared detection using an Automated Infrared Inorganic Carbon Analyzer by Marianda; TA was analyzed using an open-cell potentiometric titration (with components from Metrohm), both following established best practices (Dickson et al., 2007). Analysis of certified reference materials from A. G. Dickson (Scripps Institution of Oceanography) ensured that the uncertainty (accuracy and precision) of the TCO_2 and TA measurements was better than 2 and 3 μmol/kg, respectively.

3.3. pH Sensor Calibration

Using the standard set of carbonate system equations, TCO_2 and TA measurements alongside the pH sensor were used to compute $pH_{discrete}$ using CO2SYS (van Heuven et al., 2011), with the carbonic acid dissociations constants from Mehrbach et al. (1973) refit by Dickson and Millero (1987). The pH sensor data were calibrated with the discrete samples; the accuracy of the pH sensor data is estimated to be ±0.02 (see Figure 2) and is presented on the total scale. It is now well known that organic acid anions in dissolved organic material contribute to TA in many rivers, and the use of TA in CO_2 system computations biases the estimates of derived parameters (Abril et al., 2015; Hunt et al., 2011; Wang et al., 2013). There are no direct organic alkalinity estimates for the Chesapeake Bay. The shelf waters of the eastern United States have a mean organic alkalinity of less than 10 μmol/kg (Patsavas et al., 2015), which would result in a bias on the order of 0.03 in pH computed on the basis of TCO_2 and TA, which would be propogated through to the sensor data calibrated using the discrete samples. We assume the error associated with the sensor pH is 0.03.

3.4. Computed High-Frequency CO_2 System Parameters

The continuous pH, temperature, and salinity time series from the SeapHOx deployments were combined with the discrete TCO_2 and TA measurements to construct continuous time series of TA, TCO_2, pCO_2, and Ω_{ar} in three steps. First, a linear relationship between TA and salinity was derived from discrete samples collected at the location of the sensor (see Figure 3). These data include samples collected during the two deployments (n=8), as well as those collected outside of the D1 and D2 time periods (n=7) to robustly characterize the location in terms of its relationship between TA and salinity. Second, this relationship was used to compute a time series of TA from the daily-averaged salinity data measured by the SeapHOx sensor (e.g., Shadwick et al., 2011). Third, the TA and pH were used to compute corresponding time series of TCO_2, pCO_2 and Ω_{ar} using the CO2SYS as described above. We estimated the root mean square error in the TA time series (eTA = 8 μmol/kg) from the fit of the linear relationship. Given the errors in the sensor pH (see section 3.3) and computed TA, errors in the computed time series of TCO_2 ($eTCO_2$ = 12 μmol/kg), pCO_2 ($epCO_2$ = 20 μatm), and Ω_{ar} ($e\Omega_{ar}$ = 0.06) were estimated using the error propagation package of Orr et al. (2018).

3.5. Partitioning of CO_2 System Changes

The changes in TCO_2 at the York River location are caused by a combination of circulation (advection and mixing), air-sea CO_2 exchange, and biological processes (photosynthesis and respiration):

$$\Delta TCO_2^{obs} = \Delta TCO_2^{circ} + \Delta TCO_2^{gas} + \Delta TCO_2^{bio}, \quad (1)$$

where ΔTCO_2^{obs} is the observed change (relative to the initial conditions on the first day of the deployment), ΔTCO_2^{circ} and ΔTCO_2^{gas} are computed quantities (as detailed below), and ΔTCO_2^{bio} is computed by difference from the above equation. Based on the near-conservative relationship between observed salinity and TA (Figure 3), we assume that calcification can be neglected in this analysis.

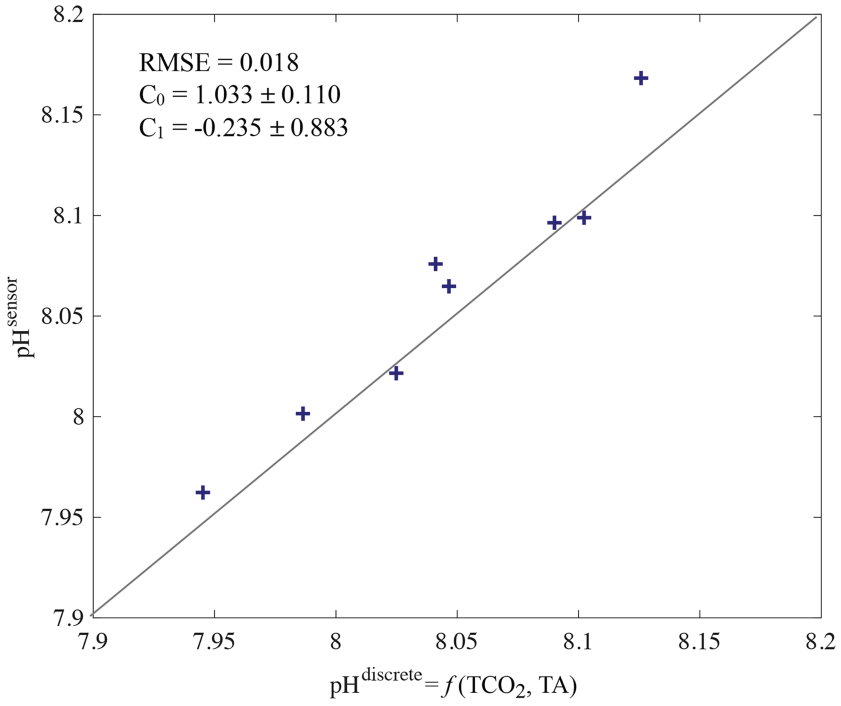

Figure 2. Discrete pH computed from TCO_2 and TA samples compared to uncalibrated sensor pH (n=8); all samples are from surface waters at the York River Buoy location. The solid line represents a 1:1 relationship (i.e., $pH^{sensor} = pH^{discrete}$); c_0 and c_1 are the sensor of the least squares fit of pH^{sensor} versus $pH^{discrete}$. RMSE = root mean square error; TA = total alkalinity.

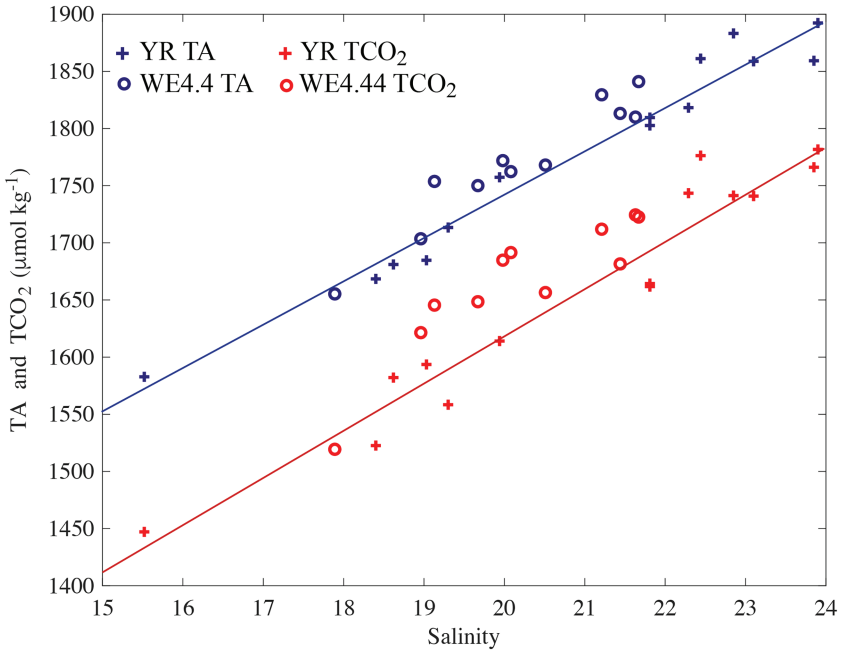

Figure 3. Relationship between surface salinity and TA (blue +) and salinity and TCO_2 (red +) measured at the York River buoy location between June 2016 and July 2018. Linear regression of the TA and salinity yields the equation TA = 37 S + 995 (n=15,r^2 = 0.96, error associated with the fit is 8 μmol/kg); linear regression of the TCO_2 and salinity yields the equation TCO_2 = 41 S + 794 (n=15,r^2 = 0.89, error associated with the fit is 12 μmol/kg). Data from the nearby Station WE4.4 (open circles) are also shown. TA = total alkalinity.

We estimate the changes due to circulation with the following equation:

$$\Delta TCO_2^{circ} = m\Delta S, \quad (2)$$

where m is the slope of the linear fit to discrete samples of TCO_2 and salinity at the sensor location (see Figure 3), and ΔS is the difference between the observed salinity and the baseline value on the first day of the deployment. The error associated with this term (12 μmol/kg) is assumed equal to the error in the fit of TCO_2 to salinity.

The TCO_2 at the sensor is assumed to be representative of the TCO_2 of the mixed layer. Thus, ΔTCO_2^{gas} is equal to $-F_{CO2}/h$, where h is the mixed-layer depth and F_{CO2} is the air-sea CO_2 flux. The mixed layer was assumed to be a constant depth of 4 m based on the definition provided in Irby et al. (2016). This method assumes that stratification occurs if there is a 10% change in the difference between the maximum and minimum densities within a 1-m bin; the mixed-layer depth is defined as the shallowest occurrence of this change.

The air-sea CO_2 flux was computed using the conventional flux equation

$$F_{CO2} = k\alpha(pCO_2 - pCO_2^{atm}), \quad (3)$$

where k and α are the gas transfer velocity and the coefficient of solubility (Weiss, 1974), respectively, pCO_2 is the surface water pCO_2 and pCO_2^{atm} is the atmospheric pCO_2. The gas transfer velocity was computed using the formulation of Wanninkhof (2014), that is, $k = 0.251\ U^2\ (Sc/660)^{0.5}$, where k has units of cm hr $^{-1}$, U^2 is the wind speed at a height of 10 m above the sea surface in units of m s^{-1}, and Sc is the Schmidt number for CO_2. A negative flux indicates a transfer from the atmosphere to the ocean. A constant value of atmospheric CO_2 of 407 μatm, the 2017 mean from the World Data Centre for Greenhouse Gases station in Key Biscayne, Florida, the longest nearby record of frequent sampling of atmospheric CO_2, is used. The 2018 data were not available, and thus, the 2017 mean is used for both deployments. The surface water pCO_2 is much more variable than the atmospheric values, and therefore, the air-sea fluxes are relatively insensitive to the use of a single mean atmospheric CO_2 concentration.

Because of gaps in the wind speed data at the York River Buoy, wind speeds were obtained from the North American Mesoscale (NAM) forecast system and averaged to a daily resolution. Comparison of available wind speed data from the York River Buoy with the NAM product indicates that both the variability and the range of values is captured by the wind forecast (n=85, $RMSE$ = 2.9 m/s, and bias = 0.5 m/s). We assume that the error associated with the air-sea flux is 20% and stems largely from the uncertainty in the gas transfer velocity (Wanninkhof, 2014), but note that this is likely to be a minimum estimate of the uncertainty given the error associated with the fit between the two sources of wind speed data. This corresponds to an error of 15 μmol/kg on the ΔTCO_2^{gas} term.

The changes in mixed-layer TCO_2 due to biology were then computed by difference; the uncertainty associated with ΔTCO_2^{bio} (23 μmol/kg) is estimated by propagating the uncertainties associated with the other terms in equation (1), assuming the uncertainties are uncorrelated (i.e., $(12^2+12^2+15^2)^{0.5}$=23).

While changes in pCO_2, pH, and Ω_{ar} can be attributed to changes in circulation, gas exchange, and biological processes through the impact of these processes on TCO_2 and TA, additional impacts of temperature and salinity must be considered. Changes in pCO_2 (and pH and Ω_{ar}) due to changes in TCO_2, TA, salinity, and temperature (i.e., $\partial pCO_2/\partial TCO_2$, $\partial pCO_2/\partial TA$, $\partial pCO_2/\partial S$, and $\partial pCO_2/\partial T$) are nonlinear, but if the variability of TCO_2, TA, salinity, and temperature is relatively small, the effects of the nonlinearity on the pCO_2 (and pH and Ω_{ar}) are also small. Thus, for example, changes in pCO_2 are given by

$$\Delta pCO_2^{obs} = \Delta pCO_2^{circ} + \Delta pCO_2^{gas} + \Delta pCO_2^{bio} + \Delta pCO_2^{temp} + \Delta pCO_2^{sal} + \epsilon, \quad (4)$$

where ϵ is the error or residual (computed by difference from the observations and the sum of all other terms in equation (4)), which stems from the nonlinear effect in the analysis described above.

The changes in pCO_2 (and pH and Ω_{ar}) are computed by assuming that each process acted on the carbonate system while other variables are held constant (Jiang et al., 2013; Shadwick et al., 2015; Wang et al., 2017).

The changes due to circulation are computed by assuming that circulation influences salinity, TA, and TCO_2 but not temperature. Salinity and TA are assumed to vary as observed, while TCO_2 is assumed to vary according to ΔTCO_2^{circ}. The changes due to air-sea CO_2 exchange are computed by allowing the TCO_2 to vary using ΔTCO_2^{gas}, while TA, salinity, and temperature are held constant at their initial values. The changes due to biology are computed by allowing the TCO_2 to vary using ΔTCO_2^{bio}, while TA, salinity, and temperature are held constant at their initial values. In the case of pCO_2 (and pH and Ω_{ar}; see equation (4)), changes due to temperature are computed by allowing the temperature to vary as observed, while TCO_2, TA, and salinity are held constant at their initial values. Finally, for pCO_2 (and pH and Ω_{ar}), the changes due to the impact of salinity on the equilibrium constants are computed by allowing the salinity to vary as observed, while TCO_2, TA, and temperature are held constant at their initial values.

3.6. Long-Term Measurements

Hydrographic conditions in the York River tributary during the sensor deployments were characterized using long-term measurements of streamflow from U.S. Geological Survey (USGS) gauges in the Mattaponi (USGS Station 01674500) and Pamunkey (USGS Station 01673000) rivers. The York River estuary also receives freshwater from several smaller rivers as well as from groundwater; approximately 35% of the York River basin is located below USGS gauging stations (Seitz, 1971).

The Chesapeake Bay Program has been monitoring temperature, salinity, and pH at Station WE4.4 since 1984 (Figure 1). A profile of 1- to 2-m depth resolution is made twice per month in May, June, July, August, and September and monthly throughout the remainder of the year. The pH measurements are made with a YSI sensor calibrated with buffer solutions of pH = 7 and pH = 10 before and after the survey (EPA, 1996). The accuracy of the pH measurements is estimated by the manufacturer to be 0.1. Monthly climatologies of T, S, and pH were constructed to place our field deployments into a historical context. Since the Chesapeake Bay Program pH are reported on the NBS scale, TA was computed from the relationship between TA and S presented above and used to convert these data to the total scale for comparison with the continuous SeapHOx pH data.

4. Results

4.1. New pH Observations in the Context of the Long-Term Record

Streamflow is generally presented in water years (WY; from October to September), and therefore, D1 was in WY2017 and D2 was in WY2018 (Figure 4a). Relative to the long-term climatology, WY2017 (D1) was relatively dry, while WY2018 (D2) was relatively wet, particularly in the autumn and summer seasons. Comparison of the salinity observed throughout D1 and D2 (i.e., between November 2016 and June 2018), with the climatological records from nearby Station WE4.4, indicates that the transition from winter to spring is broadly similar in terms of hydrography; the salinity generally decreases throughout the deployments, with a maximum salinity of 24.8 in winter decreasing to 15 in the spring and early summer seasons (Figure 4b). The sensor data indicate higher salinity during D1, consistent with lower streamflow (Figure 4a). During D2, the salinity is lower than the long-term mean at the end of the record, which is consistent with elevated flows throughout WY2018; considering the relationship between residence time and streamflow, a lag of 45 to 90 days from the upper watershed to the York River Buoy is expected (Reay, 2009; Shen & Haas, 2004). There is significant seasonality in water temperature with values near 0 °C in winter and approaching 30 °C in summer (Figure 4c). The temperature during D1 was broadly consistent with the long-term mean, while the D2 temperatures were lower for the majority of the deployment.

The winter pH in D1, from late November to March, ranged from a minimum of 7.95 to a maximum of 8.18 (mean pH of 8.06 and standard deviation 0.05), after which the pH declined steadily to minimum values approaching 7.9 in early April, followed by a modest increase until the end of the time series (Figure 4d). The pH was more variable during D2 (mean 8.09 and standard deviation 0.10): The late-December and early-January pH was 7.98 and increased steadily from mid-January until mid-April, when a sharp decline from roughly 8.32 to less than 7.95 in late-April was observed (Figure 4d). This was followed by a rapid increase between early May and the end of the record in early June to a pH of 8.31.

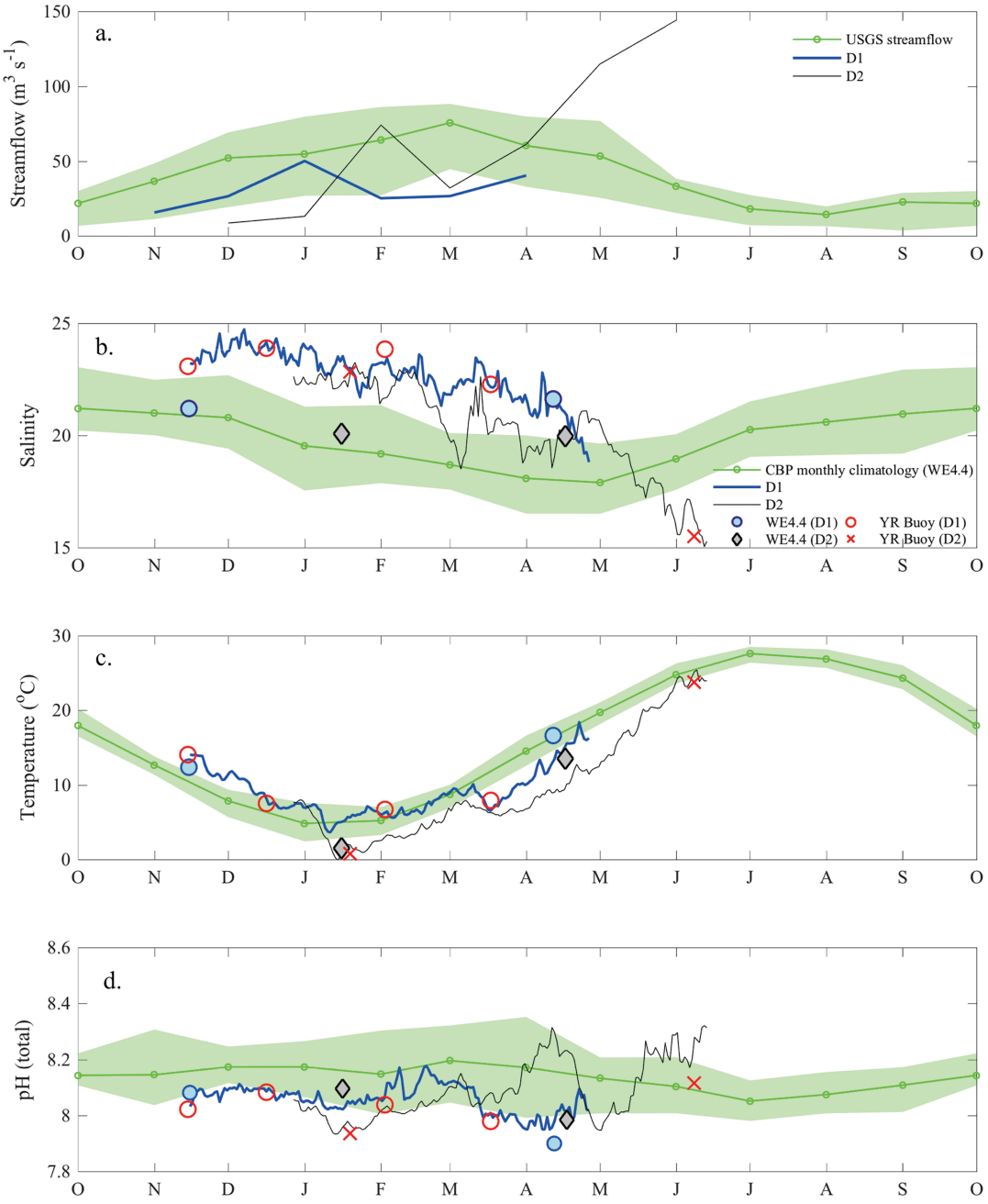

Figure 4. Long-term discharge data, long-term discrete observations from the Chesapeake Bay Program (CBP) Monitoring Station WE4.4, and sensor data from the York River site in 2016–2018: (a) discharge from the USGS Mattaponi and Pamunkey River gauges, (b) salinity, (c) temperature, and (d) pH. In (a), the long-term monthly discharge is shown as well as the quartiles of the 1989 to 2018 mean (green shaded area) and discharge over Deployment Periods D1 (blue) and D2 (black). In (b)–(d), the climatological mean (open symbols) and the quartiles of the 1984–2018 mean (shaded area) from Station WE4.4 are shown in green; lines indicate sensor data from D1 (blue) and D2 (black) at the York River Buoy; discrete samples collected at Station WE4.4 during the sensor deployments are shown as blue circles (D1) and gray diamonds (D2); samples collected at the York River Buoy during sensor deployments are shown as red circles (D1) and red X's (D2). The annual cycles of the long-term data has been plotted as water year from October to October and to line up with the timing of sensor deployments. All data shown are from surface waters. USGS = U.S. Geological Survey.

4.2. Winter-to-Spring CO_2 System Variability

The evolution of TA mirrors that of salinity during both deployments, with overall declining concentrations from initial values of 1,870 (D1) and 1,820 μmol/kg (D2) to minimum values of less than 1,700 μmol/kg in D1 and less than 1,600 μmol/kg in D2, corresponding to salinity minima (Figure 5a). This decline was overlaid

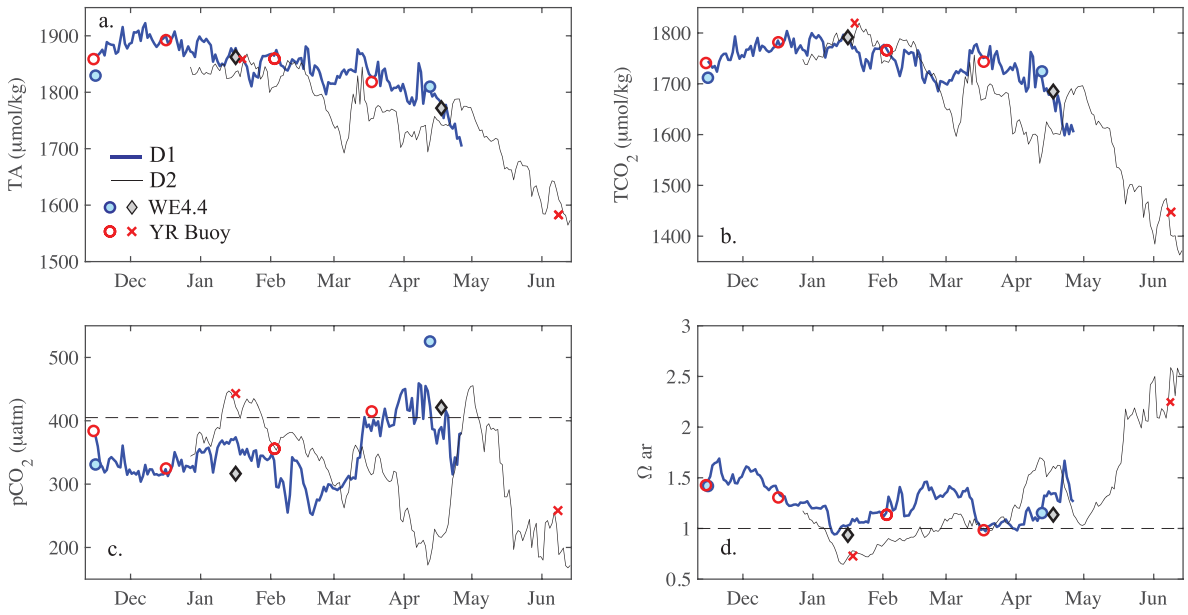

Figure 5. CO_2 system parameters at the York River Buoy: (a) TA, (b) TCO_2, (c) pCO_2, and (d) Ω_{ar}. Sensor data from Deployment 1 (D1; 2016/2017) are shown in blue and from Deployment 2 (D2; 2017/2018) in black. Red circles (and X's) indicate discrete samples collected at the York River Buoy during D1 (and D2). Blue circles (2016/2017) and gray diamonds (2017/2018) indicate discrete observations from the nearby Station WE4.4. In the case of the sensor data, pH and TA are used to derive the TCO_2, pCO_2, and Ω_{ar} time series for the two deployments. In the case of the discrete data, TA and TCO_2 measurements are used to derive the pH, pCO_2, and Ω_{ar}. The dashed lines in (c) and (d) indicate the atmospheric CO_2 concentration (407 µatm) and a saturation state of Ω_{ar}=1.0, respectively. TA = total alkalinity.

by higher-frequency changes of up to 150 µmol/kg (e.g., between mid-February and early March in D2). During D1, there was a correspondingly steady concentration of TCO_2 ranging from 1,760 to 1,800 µmol/kg between mid-November and mid-February and then a decline from mid-March until the end of the time series, with a minimum concentration of 1,600 µmol/kg (Figure 5b) at the very end of the deployment. The TCO_2 in D2 closely mirrored the seasonal change in salinity, decreasing sharply between mid-February and early March from roughly 1,800 µmol/kg to less than 1,600 µmol/kg (Figure 5b). This decline was followed by a more rapid increase in early March, overlaid with higher-frequency variability ranging from 20 to 50 µmol/kg, followed by a decline to a minimum of less than 1,400 µmol/kg coincident with a minimum salinity of 15 (Figure 5b).

During D1, there were brief periods of pCO_2 supersaturation with respect to the atmosphere in March and April (Figure 5c), and the carbonate saturation state remained in the range of Ω_{ar}=1.0 to 1.5, with minima observed in mid-January and mid-March (Figure 5d). The pCO_2 declined until mid-April in D2, followed by a rapid increase to values greater than the atmospheric concentration at the end of April, and then a rapid decrease to minimum values of 200 µatm in June (Figure 5c). High-frequency variability (days to weeks) in pCO_2 results in changes up to of 50 µatm. During D2, between April and May 2018, the pCO_2 increased from less than 200 µatm to greater than 400 µatm in less than a month. The saturation state in D2 broadly tracked the changes in pH, with winter minima of Ω_{ar}<1.0 in January, and steady increases, interrupted by a short-lived decline in late April, reaching values of 2.5 in June, coincident with the temperature maximum and salinity minimum (Figure 5d).

4.3. Air-Sea CO_2 Flux

Wind speeds were similar during the two deployments, with values ranging from less than 5 m/s with periodic increases to speeds exceeding 10 m/s but with no real defined seasonality (Figure 6). The air-sea fluxes were broadly similar between deployments, with uptake of CO_2 by the surface ocean through the majority of the time series. The mean flux in D1 was −5.0 mmol $C \cdot m^{-2} \cdot day^{-1}$, with a standard deviation of 6.7 mmol $C \cdot m^{-2} \cdot day^{-1}$; the mean flux in D2 was −8.6 mmol $C \cdot m^{-2} \cdot day^{-1}$ with standard deviation of 12.5 mmol $C \cdot m^{-2} \cdot day^{-1}$. There were brief episodes of outgassing observed in April 2017 (D1), and in late

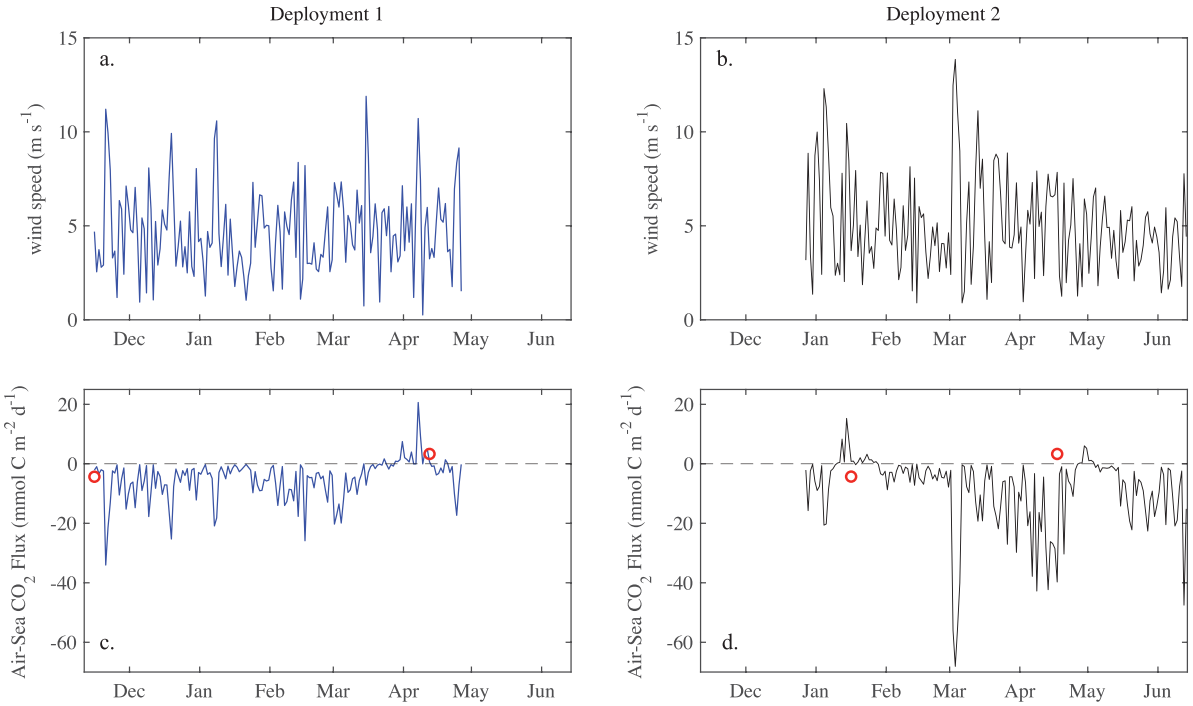

Figure 6. Wind speed (a,b) and air-sea CO_2 flux (c,d) in D1 (a,c) and D2 (b,d). The fluxes computed from the discrete samples collected at Station WE4.4 are indicated by the red circles in the bottom two panels. Winds are from the North American Mesoscale forecast system (https://www.ncdc.noaa.gov/data-access/model-data/model-datasets/north-american-mesoscale-forecast-system-nam).

January and early May 2018, and a particularly large influx of CO_2 in March 2018 coincident with an enhancement of both the pCO_2 undersaturation and the wind, with speeds approaching 15 m/s.

4.4. Physical and Biological Drivers of CO_2 System Changes

Figures 7 and 8 show the decomposition of TCO_2, pCO_2, pH, and Ω_{ar} with respect to circulation, biology, and air-sea CO_2 exchange. Also shown are the impacts of temperature, salinity, and the residual due to the nonlinearity of the carbonate system on pCO_2, pH, and Ω_{ar}. What emerges is that all processes are needed to explain how the CO_2 system varies at the study site. The nonlinear term is seen to be modest, justifying our assumption of constant derivatives of pCO_2, pH, and Ω_{ar} with respect to TCO_2, TA, temperature, and salinity. The individual impacts of circulation, temperature, air-sea CO_2 exchange, salinity, and biology on the CO_2 system are discussed in detail below.

The CO_2 system of the lower York River is strongly influenced by changes in circulation, as seen in particular with the seasonal decreases in TCO_2 between March and June 2018 (Figure 5b). The circulation-driven changes in TCO_2 dominated the other drivers in both deployments (Figures 7a and 8a), with net decreases due to circulation in D1 and D2. The decrease in TCO_2 results in a decrease in pCO_2, while the decrease in TA would increase the pCO_2; the overall decrease in pCO_2 in both D1 and D2 (Figures 7b and 8b) due to circulation indicates a dominance of TCO_2 over TA. Similarly, the overall increases in pH and Ω_{ar} due to circulation (Figures 7c, 7d, 8c, and 8d) are due to the dominance of a decrease in TCO_2, with the decrease in TA playing a more minor role.

The air-sea flux of CO_2 made the smallest contribution to TCO_2 during both deployments, with a few brief periods of outgassing decreasing TCO_2, and uptake of CO_2 increasing TCO_2 (Figures 7a and 8a). The changes due to salinity alone on pCO_2, pH, and Ω_{ar} were modest in both deployments (20 μatm pCO_2, 0.05 in pH, and <0.1 in Ω_{ar}; Figures 7 and 8, panels c and d). In D1, the contribution was neutral until early March, when it decreased the pCO_2 by 10 μatm and increased pH and Ω_{ar} by 0.2, and 0.05, respectively, until the end of the time series. In D2, there was a similarly neutral contribution from salinity until early March and a

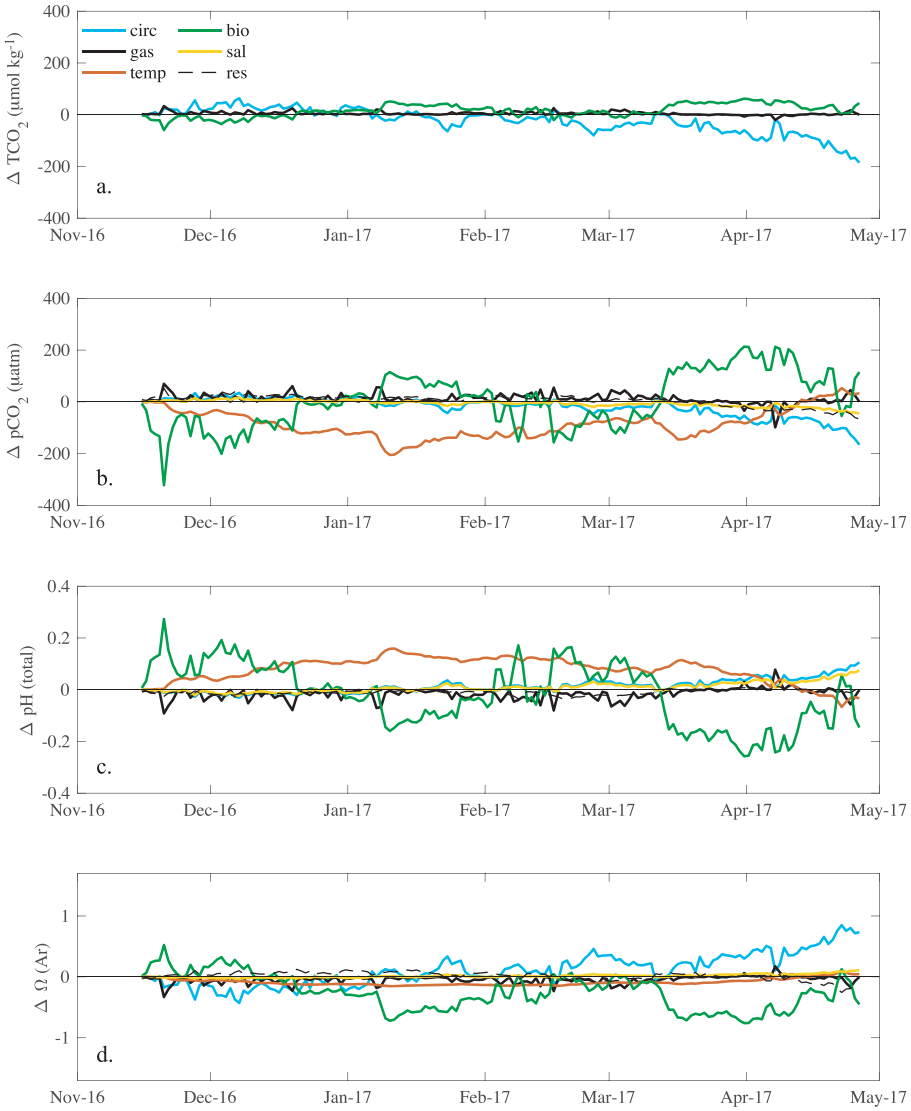

Figure 7. Partitioning across physical and biological controls on the CO_2 system during D1: (a) changes in TCO_2, (b) pCO_2, (c) pH, and (d) Ω_{ar}. Changes due to circulation (circ) are in blue, gas exchange (gas) are in black, temperature (temp) are in orange, biology (bio) are in green, salinity (sal) are in yellow, and the residual due to the nonlinearity of the carbonate system (res) is shown by the blacked dashed line.

subsequent decrease in pCO_2 (increase in pH and Ω_{ar}), roughly double the magnitude seen in D1, consistent with the larger freshening of the water in spring and summer during D2 (Figures 4b and 8b–8d).

Temperatures generally decreased from November to mid-January (Figure 4c), driving decreases in pCO_2 and increases in pH but with very little influence on Ω_{ar} (Figures 7 and 8, panels b–d). A reversal of this process occurred in mid-April in D1 and in early April in D2, when warming of the surface waters resulted in increased pCO_2 and decreased pH. This thermal increase was up to 100 μatm (decrease up to 0.2 in pH) and extended into the early summer season in D2. As was the case for TCO_2, the air-sea exchange of CO_2 makes the smallest contribution to changes in pCO_2, pH, and Ω_{ar} (Figures 7 and 8, panels c and d).

The negative change in the biological component of the changes in TCO_2 indicates a dominance of photosynthesis early in the D1 time series, with a reversal in late December when respiration dominates until an equilibrium is reached (i.e., cumulative photosynthesis = cumulative respiration, $\Delta TCO_2^{bio} \sim 0$) between early February and mid-March (Figure 7a). From mid-March until the end of the D1 time series, respiration again dominates with increases in TCO_2 due to biology of up to 80 μmol/kg coincident with a period of

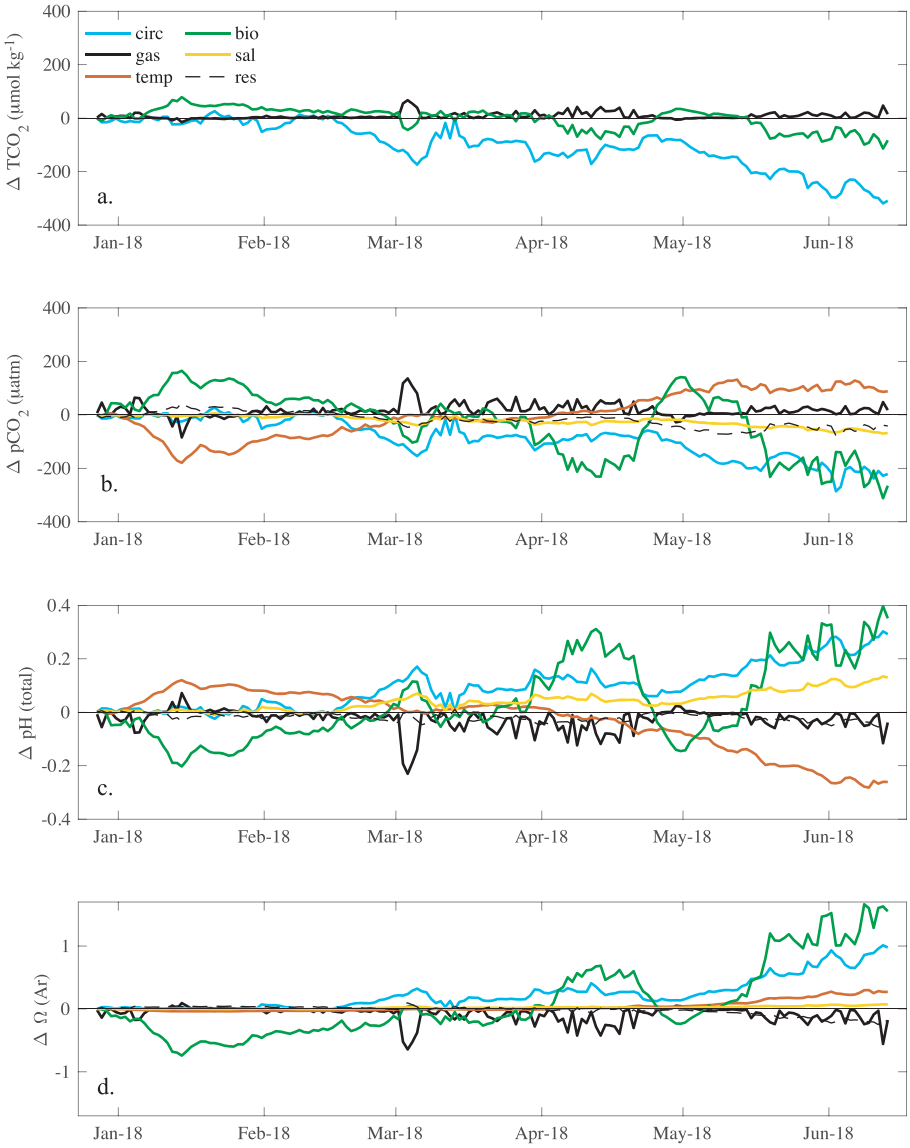

Figure 8. Partitioning across physical and biological controls on the CO_2 system during D2: (a) changes in TCO_2, (b) pCO_2, (c) pH, and (d) Ω_{ar}. Changes due to circulation (circ) are in blue, gas exchange (gas) are in black, temperature (temp) are in orange, biology (bio) are in green, salinity (sal) are in yellow, and the residual due to the nonlinearity of the carbonate system (res) is shown by the blacked dashed line.

decreased TCO_2 due to circulation. These patterns are mirrored in the biological component of changes in pCO_2 (Figure 7b), with biology decreasing pCO_2 by up to 300 μatm in late autumn (increasing pH and Ω_{ar} by nearly 0.3, and 0.5, respectively; Figures 7c and 7d) and increasing pCO_2 by greater than 200 μatm (decreasing pH and Ω_{ar} by 0.2, and 0.5, respectively) in the spring season.

The biological component in D2 evolves somewhat differently (Figure 8a), with a transition from respiration-dominated conditions in winter to a dominance of photosynthesis at the beginning of March. The biologically driven decreases in TCO_2 (and pCO_2; Figure 8b) are short lived, with neutral conditions developing in early March and persisting for roughly a month, before production again dominates, decreasing pCO_2 by 200 μatm in April. This is followed by a rapid biologically driven increase in pCO_2 (and a correspondingly rapid decrease in pH and Ω_{ar}; Figures 8c and 8d) indicating a shift to respiration exceeding production in the middle of the typical spring season. In mid-May, this reverses again, and photosynthesis dominates the biologically driven changes for the remainder of the record. This results in large enhancements in both pH and

Ω_{ar}, outweighing the decrease in pH due to warming, and combining with the small thermal enhancement in Ω_{ar}. This dominance of biologically mediated changes in TCO_2 on changes in Ω_{ar} was similarly reported in the Gulf of Maine by Wang et al. (2017) during the spring-to-summer transition in that system. However, the distinct evolution of the biological component of CO_2 system changes between deployments observed here indicates that interannual variability is significant and a single period of observations over a seasonal transition may be insufficient to characterize the system dynamics.

5. Discussion

5.1. High-Frequency Versus Seasonal Sampling

The hydrographic and CO_2 system data from the sensor are compared to discrete samples collected on seasonal cruises: two samples were collected in the region over the period of D1 in 2016 and 2017, and two samples were collected over the D2 period in 2017 and 2018 (Figures 4 and 5). The seasonality in temperature is well represented by the discrete seasonal sampling, while the salinity at the York River site was higher than that at Station WE4.4 in autumn and early winter but consistent at the time of discrete sampling at Station WE4.4 in April in both years (Figures 4b and 4c). The station data indicate that pH is similar between the two locations, but as expected, higher-frequency changes in pH are not well captured by the seasonal sampling (Figure 4d).

There is a good agreement between the discrete TA and the sensor TA computed via a relationship with salinity (Figure 5a). The TCO_2 is similarly well represented by the sparse discrete sampling at the station (Figure 5b). The discrete pCO_2 data indicate undersaturation with respect to the atmosphere in autumn and winter with the brief period of supersaturation in early April 2017 captured by both the sensor and discrete data (Figure 5c). The single 2018 spring discrete sample indicates modest supersaturation, while the sensor data indicates a 100-μatm gradient in pCO_2. The winter-to-summer transition from Ω_{ar} near 1.0 to values greater than 1.5 appears to be well captured by the discrete data, and there is general agreement between the sensor and the discrete values in the autumn and winter seasons (Figure 5d).

These observations suggest that the broad patterns in CO_2 system changes from one season to the next are captured by sampling with monthly or sparser resolution (see also Brodeur et al., 2019); however, attribution of the drivers of those changes to particular physical and/or biological processes is more robust with higher-frequency observations. Furthermore, the discrete seasonal sampling does not allow the air-sea CO_2 flux to be captured appropriately. A comparison of fluxes computed on the basis of the discrete seasonal sampling and those computed from the continuous sensor data, using both daily and monthly averages, is given in Table 1. During D1, the discrete sampling captures the direction of the flux in November and April, but the magnitudes are quite different. During D2, the fluxes computed with discrete samples in both January and April were in the opposite direction to those computed from the daily sensor data; the magnitude of the fluxes differed by an order of magnitude. We note that the air-sea CO_2 gradient (ΔpCO_2) computed from the sensor data yields fluxes in the direction reported even when the fairly large uncertainty in the pCO_2 computed on the basis of pH and TA estimated from salinity is taken into account. This suggests that the low-frequency discrete seasonal sampling may significantly bias in situ estimates of air-sea CO_2 exchange.

5.2. CO_2 Source/Sink Status of the Lower York River

Investigations of the role of continental shelves in the uptake of atmospheric CO_2 have resulted in a broad classification of estuaries as net sources of CO_2 to the atmosphere and sources of inorganic and organic carbon to the continental shelves and coastal oceans (Borges et al., 2005; Cai et al., 2003; Chen & Borges, 2009; Flecha et al., 2015; Frankignoulle et al., 1998; Jiang et al., 2008). Sustained measurements of the CO_2 system and quantification of carbon fluxes in nearshore

Table 1
Comparison of Air-Sea CO_2 Flux Computed From Individual Discrete Samples and Continuous Sensor Data: n=1 for the Day and n=15 for Month in November 2016, n=30 for Month in April 2017 and 2018, and n=31 for Month in January 2018

	Sensor (day)	Sensor (month)	Discrete
Nov 2016	−2.1	−8.2	−4.3
Apr 2017	0.6	0.3	3.3
Jan 2018	0.8	1.4	−4.4
Apr 2018	−39.7	−14.4	3.1

environments have increased in recent years (Brodeur et al., 2019; Joesoef et al., 2015; Shadwick et al., 2010; Signorini et al., 2013; Vandemark et al., 2011), and regional budgets have been developed (Herrmann et al., 2015; Laruelle et al., 2010; Najjar et al., 2018).

The mainstem of the Chesapeake Bay is thought to be net autotrophic (Feng et al., 2015; Kemp et al., 1997) and a modest sink for atmospheric CO_2, while its tributaries may broadly be considered heterotrophic, potentially acting as sources of atmospheric CO_2 on the annual scale (Herrmann et al., 2015). The York River Estuary has previously been designated a source of atmospheric CO_2 fueled by net heterotrophy based on observations collected over a 2-year period (Raymond et al., 2000). These new observations from the lower York River and the Chesapeake Bay mainstem during the winter and spring indicate that the region acts as a sink for atmospheric CO_2 during this time period, with short-lived episodes of pCO_2 supersaturation, and may be more representative of conditions in the Chesapeake Bay mainstem than the York River estuary as a whole. The pCO_2 observed in both D1 and D2 are similar to those reported for the nearby Delaware Estuary, which experiences a similarly large seasonal change in temperature (Joesoef et al., 2015). The Delaware system is characterized by significant CO_2 outgassing in the low-salinity head waters, which are largely compensated by biologically driven CO_2 uptake in the larger lower estuary such that the system as a whole is a weak source of atmospheric CO_2 on the annual time scale (Joesoef et al., 2015).

The 2017 (D1) observations suggest that the lower York River might transition to outgassing in June and July due to significant surface water warming coincident with the decline of the spring production, though we note that these months were not captured by the data presented here. Such a transition would be similar to the seasonality observed further north in the Scotian Shelf and Gulf of Maine regions, where thermally driven increases in pCO_2 due to a temperature seasonality of similar magnitude to that observed in the York River result in weak uptake or outgassing of CO_2 to the atmosphere outside of the productive spring season (Shadwick et al., 2011; Signorini et al., 2013; Vandemark et al., 2011). However, the 2018 (D2) observations indicate much lower pCO_2, roughly 200 μatm, in waters warmer than 20°C in June, just before the end of the record, highlighting both the significant interannual variability and the role of freshwater input in controlling seasonality in the CO_2 system at this location.

6. Conclusion

Using a combination of sensor data and high-quality discrete observations, a partitioning of the CO_2 system into physical and biological drivers was established. This study shows the dominance of circulation and biological processes in CO_2 system variability over the winter-to-spring transition in the lower York River. Decreases in TCO_2 driven by freshening occur against a background of uptake of atmospheric CO_2. The surface waters remain undersaturated through the majority of both deployments from late autumn to early summer. These new observations indicate that the region may change from conditions of autotrophy (photosynthesis > respiration) to heterotrophy (respiration > photosynthesis) multiple times and that the region is not necessarily characterized by the development of a spring bloom and a transition from wintertime heterotrophy to summertime autotrophy. The biological component of the TCO_2 variability was significantly different between deployments, both with respect to the timing of the change in sign (i.e., autotrophy vs. heterotrophy) and the magnitude of the change. This variability had consequences for the pCO_2 and pH, with interactions between seasonal changes in temperature (warming increasing pCO_2 and decreasing pH), biology, and freshening (decreasing pCO_2 and increasing pH and Ω_{ar}) dominating the seasonal changes in these parameters. These results highlight the sensitivity of the CO_2 system to high-frequency changes in hydrography and biology and also the significant natural variability in the dynamic estuarine environment. This work also highlights the importance of long-term monitoring and demonstrates the utility of combining autonomous platforms with routine sampling to constrain high-frequency CO_2 system variability.

Acknowledgments
Funding was provided by the National Science Foundation via Grants OCE-1537013 and OCE-1536996. We are grateful to the NOAA Chesapeake Bay office for their assistance and collaboration. We thank Todd Martz at USCD for the SeapHOx sensor used to generate the continuous data used in this work and P. St-Laurent and M. Herrmann for their input. We are grateful to two anonymous reviewers for their constructive comments. This paper is Contribution 3840 of the Virginia Institute of Marine Science, William & Mary. Data used in the analysis are publicly available at William & Mary's ScholarWorks (https://doi.org/10.25773/63NX-VZ39).

References

Abril, G., Bouillon, S., Darchambeau, F., Teodoru, C. R., Marwick, T. R., Tamooh, F., et al. (2015). Technical note: Large overestimation of pCO_2 calculated from pH and alkalinity in acidic, organic-rich freshwaters. *Biogeosciences*, *12*, 67–78. https://doi.org/10.5194/bg-12-67-2015

Bever, A. J., Friedrichs, M. A. M., Friedrichs, C. T., Scully, M. L., & Lanerolle, L. W. J. (2013). Combining observations and numerical model results to improve estimates of hypoxic volume within the Chesapeake Bay, USA. *Journal of Geophysical Research: Oceans*, *118*, 4924–4944. https://doi.org/10.1002/jgrc.20331

Borges, A. V., Delille, B., & Frankignoulle, M. (2005). Budgeting sinks and sources of CO_2 in the coastal ocean: Diversity of ecosystems counts. *Geophysical Research Letters*, *32*, L14601. https://doi.org/10.1029/2005GL023053

Borges, A. V., & Gypens, N. (2010). Carbonate chemistry in the coastal zone responds more strongly to eutrophication than to ocean acidification. *Limnology and Oceanography*, *55*(1), 346–353.

Boynton, W. R., Garber, J. H., Summers, R., & Kemp, W. M. (1995). Inputs, transformations, and transport of nitrogen and phosphorus in Chesapeake Bay and selected tributaries. *Estuaries*, *18*, 285–314.

Bresnahan, P. J., Martz, T. R., Takeshita, Y., Johnson, K. S., & LaShomb, M. (2014). Best practices for autonomous measurement of seawater pH with the Honeywell Durafet. *Methods in Oceanography*, *9*, 44–60.

Brodeur, J. R., Chen, B., Su, J., Xu, Y.-Y., Hussain, N., Scaboo, K. M., et al. (2019). Chesapeake Bay inorganic carbon: Spatial distribution and seasonal variability. *Fontiers in Marine Science*, *6*, 99. https://doi.org/10.3389/fmars.2019.00099

Cai, W.-J. (2011). Estuarine and coastal ocean carbon paradox: CO_2 sinks of sites of terrestrial carbon incineration? *Annual Reviews of Marine Science*, *3*, 123–145.

Cai, W.-J., Huang, W.-J., Luther, G. W., Pierrot, D., Li, M., Testa, J., et al. (2017). Redox reactions and weak buffering capacity lead to acidification in the Chesapeake Bay. *Nature Communications*, *8*(1), 369. https://doi.org/10.1038/s41467-017-00417-7

Cai, W.-J., Wang, Z. A., & Wang, Y. (2003). The role of marsh-donimated heterotrophic continental margins in transport of CO_2 between the atmosphere, the land-sea interface and the ocean. *Geophysical Research Letters*, *30*(16), 1849. https://doi.org/10.1029/2003GL017633

Chen, C.-T. A., & Borges, A. V. (2009). Reconciling opposing views on carbon cycling in the coastal ocean: Continental shelves as sinks and near-shore ecosystems as sources of atmospheric co_2. *Deep Sea Research Part II*, *33*, L12603. https://doi.org/10.1016/j.dsr2.2009.01.001

Da, F., Friedrichs, M. A. M., & St-Laurent, P. (2018). Impacts of atmospheric nitrogen deposition and coastal nitrogen fluxes on oxygen concentrations in Chesapeake Bay. *Journal of Geophysical Research: Oceans*, *123*, 5004–5025. https://doi.org/10.1029/2018jc014009

Dickson, A. G., & Millero, F. J. (1987). A comparison of the equilibrium constants for the dissociation of carbonic acid in seawater media. *Deep-Sea Research Part II*, *34*, 1733–1743.

Dickson, A. G., Sabine, C. L., & Christian, J. R. (Eds.) (2007). *Guide to best practices for ocean CO_2 measurement Edited by* Dickson, A. G., Sabine, C. L., & Christian, J. R.Sidney, British Columbia:PICES Special Publication 3.

Doney, S. C., Fabry, V. J., Feely, R. A., & Kleypas, J. A. (2009). Ocean acidification: The other CO_2 problem. *Annual Reviews of Marine Science*, *1*, 169–192.

Du, J., Shen, J., Wang, Y. P., & Yu, X. (2018). Worsened physical condition due to climate change contributes to the increasing hypoxia in Chesapeake Bay. *Science of the Total Environment*, *630*, 707–714. https://doi.org/10.1016/j.scitotenv.2018.02.265

Duarte, C. M., Hendriks, I. E., Moore, T. S., Olsen, Y. S., Steckbauer, A., Ramajo, L., et al. (2013). Is ocean acidification an open ocean syndrome? Understanding anthropogenic impacts on seawater pH. *Estuaries and Coasts*, *36*, 221–236.

EPA (1996). Recommended guidelines for sampling and analyses in the Chesapeake Bay Monitoring Program (*143rd ed.; Tech. Rep.*): U.S. Environmental Protection Agency: Chesapeake Bay Program.

Ekstrom, J. A., Sautoni, L., Cooley, S. R., Pendleton, L. H., Waldbusser, G. G., Cinner, J. E., et al. (2015). Vulnerability and adaptation of US shellfisheries to ocean acidification. *Nature Climate Change*, *5*, 207–214.

Feely, R. A., Alin, S. R., Newton, J., Sabine, C. L., Warner, M., Devol, A., et al. (2010). The combined effects of ocean acidification, mixing, and respiration on pH and carbonate saturation in an urbanized estuary. *Estuarine, Coastal and Shelf Science*, *88*(4), 442–449. https://doi.org/10.1016/j.ecss.2010.05.004

Feely, R. A., Doney, S. C., & Cooley, S. R. (2009). Ocean acidification: Present condition and future changes in a high-CO_2 world. *Oceanography*, *22*, 36–47.

Feng, Y., Friedrichs, M. A. M., Wilkin, J., Tian, H., Yang, Q., Hofmann, E. E., et al. (2015). Chesapeake Bay nitrogen fluxes derived from a land-estuarine-ocean biogeochemical modeling system: Model description, evaluation and nitrogen budgets. *Journal of Geophysical Research: Biogeosciences*, *120*, 1666–1695. https://doi.org/10.1002/2015JG002931

Flecha, S., Huertas, I. E., Navarro, G., Morris, E. P., & Ruiz, J. (2015). Air-water CO_2 fluxes in a highly heterotrophic estuary. *Estuaries and Coasts*, *38*, 2295–2309. https://doi.org/10.1007/s12237-014-9923-1

Frankignoulle, M., Abril, G., BOrges, A., Bourge, I., Canon, C., Delille, B., et al. (1998). Carbon dioxide emission from European estuaries. *Science*, *282*, 434–436.

Goldsmith, K. A., Lau, S., Poach, M. E., Sakowicz, G. P., Trice, T. M., Ono, R. C., et al. (2019). Scientific considerations for optimizing acidification monitoring in the U.S. Mid-Atlantic Bight. *Estuarine, Coastal and Shelf Science*, *225*, 106189. https://doi.org/10.1016/j.ecss.2019.04.023

Gonski, S. F., Cai, W.-J., Ullmand, W. J., Joesoef, A., Main, C. R., Pettay, D. T., & Martz, T. R. (2018). Assessment of the suitability of Durafet-based sensors for pH measurement in dynamic estuarine environments. *Estuarine, Coastal and Shelf Science*, *200*, 152–168. https://doi.org/10.1016/j.ecss.2017.10.20

Haas, L. (1977). The effect of the spring-neap tidal cycle on the vertical salinity structure of the James, York and Rappahannock Rivers, Virginia. *Estuarine and Coastal Marine Science*, *5*, 485–496.

Herrmann, M., Najjar, R. G., Kemp, W. M., Alexander, R. B., Boyer, E. W., Cai, W.-J., et al. (2015). Net ecosystem production and organic carbon balance of U.S. East Coast estuaries: A synthesis approach. *Global Biogeochemical Cycles*, *29*, 96–111. https://doi.org/10.1002/2013GB004736

Hofmann, G. E., Smith, J. E., Johnson, K. S., Send, U., Levin, L. A., Micheli, F., et al. (2011). High-frequency dynamics of ocean pH: A multi-ecosystem comparison. *PLoS One*, *6*(12), e28983.

Hunt, C. W., Salisbury, J. E., & Vandemark, D. (2011). Contribution of non-carbonate anions to total alkalnity and overestimation of pCO_2 in New England and New Brunswick rivers. *Biogeosciences*, *8*, 3069–3076. https://doi.org/10.5194/bg-8-3069-2011

Irby, I. D., & Friedrichs, M. A. M. (2019). Evaluating confidence in the impact of regulatory nutrient reduction on Chesapeake Bay water quality. *Estuaries and Coasts*, *42*(1), 16–32. https://doi.org/10.1007/s12237-018-0440-5

Irby, I. D., Friedrichs, M. A. M., Friedrichs, C. T., Bever, A. J., Hood, R. R., Lanerolle, L. W. J., et al. (2016). Challenges associated with modeling low-oxygen waters in Chesapeake Bay: A multiple model comparison. *Biogeosciences*, *13*, 2011–2028. https://doi.org/10.5194/bg-13-2011-2016

Jiang, L.-Q., Cai, W.-J., & Wang, Y. (2008). A comparative study of carbon dioxide degassing in river- and marine-dominated estuaries. *Limnology and Oceanography*, *53*(6), 2603–2615.

Jiang, Z.-P., Hydes, D. J., Tyrrell, T., Hartman, S. E., Hartman, M. C., Dumousseaud, C., et al. (2013). Key controls on the seasonal and interannual variations of the carbonate system and air-sea CO_2 flux in the Northeast Atlantic (Bay of Biscay). *Journal of Geophysical Research: Oceans*, *118*, 785–900. https://doi.org/10.1002/jgrc.20087

Joesoef, A., Huang, W.-J., Gao, Y., & Cai, W.-J. (2015). Air-water fluxes and sources of carbon dioxide in the Delaware Estuary: Spatial and seasonal variability. *Biogeosciences*, *12*(20), 6085–6101. https://doi.org/10.5194/bg-12-6085-2015

Joesoef, A., Kirchman, D. L., Sommerfield, C. K., & Cai, W.-J. (2017). Seasonal variability of the inorganic carbon system in a large coastal plain estuary. *Biogeosciences*, *14*, 4949–4963. https://doi.org/10.5194/bg-14-4949-2017

Kemp, W. M. (2005). Eutrophication of Chesapeake Bay: Historical trends and ecological interactions. *Marine Ecology Progress Series*, *303*, 1–29.

Kemp, W. M., & Boynton, W. (1992). Spatial and temporal coupling of nutrient inputs to estuarine primary production: The role of particulate transport and decomposition. *Bulletin of Marine Science*, *35*, 522–535.

Kemp, W. M., Smith, E., Marvin-DiPasquale, M., & Boynton, W. (1997). Organic carbon balance and net ecosystem metabolism in Chesapeake Bay. *Marine Ecology Progress Series*, *150*, 229–248.

Laruelle, G. G., Dürr, H. H., Slomp, C. P., & Borges, A. V. (2010). Evaluation of sinks and sources of CO_2 in the global coastal ocean using a spatially-explicit typology of estuaries and continental shelves. *Geophysical Research Letters*, *37*, L15607. https://doi.org/10.1029/2010GL043691

Lin, J., & Kuo, A. (2001). Secondary turbidity maximum in a partially mixed microtidal estuary. *Estuaries*, *24*, 707–720.

Marshall, H. G. (2009). Phytoplankton of the York River. *Journal of Coastal Research*, *57*, 59–65.

Marshall, R., Lacourture, R., Buchanan, C., & Johnson, J. (2006). Phytoplankton assemblages associated with water quality and salinity regions in the Chesapeake Bay, USA. *Estuarine, Coastal and Shelf Science*, *69*, 10–18.

Martz, T. R., Connery, J. G., & Johnson, K. S. (2010). Testing the Honeywell Durafet for seawater pH applications. *Limnology and Oceanography: Methods*, *8*, 172–184.

Martz, T. R., Send, U., Ohman, M. D., Takeshita, Y., Bresnahan, P., Kim, H.-J., & Nam, S. (2014). Dynamic variability of biogeochemical ratios in the Southern California Current System. *Geophysical Research Letters*, *41*, 2496–2501. https://doi.org/10.1016/j.mio.2014.08.003

Mehrbach, C., Culberson, C. H., Hawley, J. E., & Pytkowicz, R. M. (1973). Measurement of the apparent dissociation constants of carbonic acid in seawater at atmospheric pressure. *Limnology and Oceanography*, *18*, 897–907.

Najjar, R. G., Herrmann, M., Alexander, R., Boyer, E. W., Burdige, D. J., Butman, D., et al. (2018). Carbon budget of tidal wetlands, estuaries, and shelf waters of eastern North America. *Global Biogeochemical Cycles*, *32*, 389–416. https://doi.org/10.1002/2017GB005790

Orr, J. C., Epitalon, J.-M., Dickson, A. G., & Gattuso, J.-P. (2018). Routine uncertainty propagation for the marine carbon dioxide system. *Marine Chemistry*, *207*, 84–107.

Orr, J. C., Fabry, V. J., Aumont, O., Bopp, L., Doney, S. C., Feely, R. A., et al. (2005). Anthropogenic ocean acidification over the twenty-first century and its impact on calcifying organisms. *Nature*, *437*, 681–686.

Patsavas, M. C., Byrne, R. H., Wanninkhof, R., Feely, R. A., & Cai, W.-J. (2015). Internal consistency of marine carbonate system measurements and assessment of aragonite saturation state: Insights from two U.S. coastal cruises. *Marine Chemistry*, *176*, 9–20. https://doi.org/10.1016/j.marchem.2015.06.022

Qin, Q., & Shen, J. (2019). Pelagic contribution to gross primary production dynamics in shallow areas of York River, VA, U.S.A. *Limnology and Oceanography*, *123*, 1–16. https://doi.org/10.1002/Ino.11129

Raymond, P. A., Bauer, J. E., & Cole, J. J. (2000). Atmospheric CO_2 evasion, dissolved inorganic carbon production, and net heterotrophy in the York River Estuary. *Limnology and Oceanography*, *45*, 1707–1717.

Reay, W. G. (2009). Water quality within the York River Estuary. *Journal of Coastal Research*, *57*, 23–39.

Salisbury, J. E., & Jönsson, B. F. (2018). Rapid warming and salinity changes in the Gulf of Maine alter surface ocean carbonate parameters and hide ocean acidification. *Biogeochemistry*, *141*(3), 401–418. Retrieved from https://doi.org/10.1007/s10533-018-0505-3

Seitz, R. C. (1971). Drainage area statistics for the Chesapeake Bay freshwater drainage basin (*Special Report No. 119*). Baltimore, MD: Chesapeake Bay Institute, John Hopkins University.

Shadwick, E. H., Thomas, H., Azetsu-Scott, K., Greenan, B. J. W., Head, E., & Horne, E. (2011). Seasonal variability of dissolved inorganic carbon and surface water pCO_2 in the Scotian Shelf region of the Northwestern Atlantic. *Marine Chemistry*, *124*, 23–37. https://doi.org/10.1016/j.marchem.2010.11.004

Shadwick, E. H., Thomas, H., Comeau, A., Craig, S. E., Hunt, C. W., & Salisbury, J. E. (2010). Air-sea CO_2 fluxes on the Scotian Shelf: Seasonal to multi-annual variability. *Biogeosciences*, *7*, 3851–3867.

Shadwick, E. H., Trull, T. W., Tilbrook, B., Sutton, A. J., Schulz, E., & Sabine, C. L. (2015). Seasonality of biological and physical controls on air-sea CO_2 fluxes from hourly observations at the Southern Ocean Time Series site south of Australia. *Global Biogeochemical Cycles*, *29*, 223–238. https://doi.org/10.1002/2014GB004906

Sharples, J., Simpson, J., & Brubaker, J. (1994). Observatoins and modeling of periodic stratification in the upper York River estuary. *Estuarine, Coastal and Shelf Science*, *38*, 301–312.

Shen, J., & Haas, L. (2004). Calculating age and residence time in the tidal York River using three-dimensional model experiments. *Estuarine, Coastal and Shelf Science*, *61*, 449–461. https://doi.org/10.1016/j.ecss.2004.06.010

Shen, C., Testa, J. M., Li, M., Cai, W.-J., Waldbusser, G. G., Ni, W., et al. (2019). Controls on carbonate system dynamics in a coastal plain estuary: A modeling study. *Journal of Geophysical Research: Biogeosciences*, *124*, 61–78. https://doi.org/10.1029/2018JG004802

Signorini, S. R., Mannino, A., Najjar, R. G., Friedrichs, M. A. M., Cai, W.-J., Salisbury, J., et al. (2013). Surface ocean pCO_2 seasonality and air-sea CO_2 flux estimates for the North American East Coast. *Journal of Geophysical Research: Oceans*, *118*, 5439–5460. https://doi.org/10.1002/jgrc.20369

Sunda, W. G., & Cai, W.-J. (2012). Eutrophication induced CO_2-acidification of subsurface coastal waters: Interactive effects of temperature, salinity, and atmopsheric pCO_2. *Environmental Science & Technology*, *46*, 10,651–10,659.

Sutton, A. J., Feely, R. A., Sabine, C. L., McPhaden, M. J., Takahashi, T., Chavez, F. P., et al. (2014). Natural variability and anthropogenic change in equatorial pacific surface ocean pCO_2 and pH. *Global Biogeochemical Cycles*, *28*, 131–145. https://doi.org/10.1002/2013GB004679

Takeshita, Y., Frieder, C. A., Martz, T. R., Ballard, J. R., Feely, R. A., Kram, S., et al. (2015). Including high-frequency variability in coastal ocean acidification projections. *Biogeosciences*, *12*, 5853–5870. https://doi.org/10.5194/bg-12-5853-2015

van Heuven, S., Pierrot, D., Rae, J. W. B., Lewis, E., & Wallace, D. W. (2011). Matlab program developed for CO_2 system calculations (*Tech. Rep.*): ORNL/CDIAC.

Vandemark, D., Salisbury, J. E., Hunt, C. W., Shellito, S., & Irish, J. (2011). Temporal and spatial dynamics of CO_2 air-sea flux in the Gulf of Maine. *Journal of Geophysical Research*, *116*, C01012. https://doi.org/10.1029/2010JC006408

Waldbusser, G. G., & Salisbury, J. E. (2014). Ocean acidification in the coastal zone from an organism's perspective: Multiple system parameters, frequency domains, and habitats. *Annual Reviews of Marine Science*, *6*, 221–247.

Waldbusser, G. G., Voigt, E., Bergshcnieder, H., Green, M., & Newell, R. E. (2011). Biocalcification in the eastern oyster (Crassostrea virginica) in relation to long-term trends in Chesapeake Bay pH. *Estuaries and Coasts*, *34*, 221–231.

Wallace, R. B., Baumann, H., Grear, J. S., Aller, R. C., & Gobler, C. J. (2014). Coastal ocean acidification: The other eutrophication problem. *Estuarine, Coastal and Shelf Science*, *148*, 1–13.

Wang, Z. A., Bienvenu, D. J., Mann, P. J., Hoering, K. A., Roulsen, J. R., Spencer, R. G. M., & Holmes, R. M. (2013). Inorganic carbon speciation and fluxes in the Congo River. *Geophysical Research Letters*, *40*, 511–516. https://doi.org/10.1002/grl.50160

Wang, Z. A., Lawson, G. L., Pilskaln, C. H., & Maas, A. E. (2017). Seasonal controls of aragonite saturation states in the Gulf of Maine. *Journal of Geophysical Research: Oceans*, *122*, 372–389. https://doi.org/10.1002/2016JC012373

Wanninkhof, R. (2014). Relationship between wind speed and gas exchange over the ocean revisited. *Limnology and Oceanography: Methods*, *12*(6), 351–362. https://doi.org/10.4319/lom.2014.12.351

Weiss, R. F. (1974). Carbon dioxide in water and seawater: The solubility of a non-ideal gas. *Marine Chemistry*, *2*, 203–215.

Wong, G. T. F. (1979). Alkalinity and pH in the southern Chesapeake Bay and the James River estuary. *Limnology and Oceanography*, *24*, 970–977.